Identification and minimization of errors in Doppler global velocimetry measurements

by

James F. Meyers and Joseph W. Lee

National Aeronautics and Space Administration
Langley Research Center
Hampton, Virginia 23681 USA

ABSTRACT

A systematic laboratory investigation was conducted to identify potential measurement error sources in Doppler Global Velocimetry technology. Once identified, methods were developed to eliminate or at least minimize the effects of these errors. The areas considered included the Iodine vapor cell, optical alignment, scattered light characteristics, noise sources, and the laser. Upon completion the demonstrated measurement uncertainty was reduced to 0.5 m/sec.

1. INTRODUCTION

The primary goals of the initial development phase of Doppler Global Velocimetry (DGV) were to determine the applicability of the technology to wind tunnel testing, and to find the limits of its measurement capability. Early laboratory research indicated that the potential performance of DGV could only be determined through wind tunnel testing since the conditions could not be adequately demonstrated with laboratory flow systems. Facility testing would also stress the technology with real-world engineering problems of limited viewing options, poor environmental conditions, and remote operation.

During the initial development phase a series of tests was conducted in numerous facilities in an attempt to understand the physics underlying DGV technology, along with defining the practical engineering required to apply DGV in various wind tunnel environments. These efforts led to the first DGV flow field measurements in a wind tunnel (Meyers and Komine, 1991), the first three-component DGV measurements (Usry et al, 1992), the largest planar velocity measurement area (Meyers et al, 1998), and the longest focal length of any multi-component laser velocimetry system (Usry et al, 1992).

The results from these wind tunnel investigations indicate that DGV was applicable to wind tunnel testing, and could provide three-component velocity maps of flow fields with spatial resolutions that met or exceeded the grids used in Computational Fluid Dynamics. Measurement areas were expanded to 1.5-x 1.5-meters, and focal distances lengthened to 18 meters without any degradation in performance. Investigating the flow structures of burst vortices, a hot transonic jet, and the flow above a delta wing at Mach 4.6 tested the velocity measurement capabilities (Meyers, 1994). The DGV system performed well in all cases. The high-speed investigations also tested the ability of the technology to obtain measurements from extremely small particles. The *particle lag* found during the measurement of an oblique shock using water condensation particles was traced to the Modulation Transfer Function of the cameras and not to the response of the particles to the change in velocity across the shock (Meyers, 1994). The desired goal of the initial phase to define the spatial and velocity measurement limits was not reached however.

While these results would indicate that DGV showed tremendous promise for determining three-component velocity flow fields, the initial development phase uncovered a disturbing characteristic. Although the measured velocity field appeared to be accurate in a relative sense, the data contained a significant bias error that would randomly vary from data set to data set. Attempts to determine the origin of this error during the initial phase proved unsuccessful. Thus a second development phase was started with the primary goals of identifying sources of measurement error in DGV, and then developing methods to minimize the effects of these errors.

2. APPROACH

The primary approach was to scrutinize a single-component DGV system in a controlled laboratory environment to identify system characteristics that may prove to be a weakness in the implementation of the technology. The study began by considering areas that were found to be troublesome during wind tunnel testing. Many of these areas are related to the robustness, or lack thereof, of the DGV components to the dynamic environmental conditions found in wind tunnels. Since these conditions can not be replicated in the laboratory, the effects of minor changes must be accentuated by measuring a velocity field that can be accurately determined by other means. A rotating wheel was selected to satisfy this requirement. By illuminating the wheel with a cone of laser light and placing the transmission optical axis, wheel centerline, and DGV receiver optics in a horizontal plane, only the horizontal component of velocity would be measured. Thus a linear distribution of velocity was obtained that could be determined accurately using a shaft encoder as a tachometer. A second optical receiver system was configured to monitor the optical frequency of the laser output. The simultaneous measure of the laser output and the scattered light from the rotating wheel would validate the absolute measure of velocity since there can be no Doppler shift along the horizontal wheel diameter. The laboratory setup is shown in figure 1. The laser selected for this study was an injection-seeded, frequency-doubled Nd:YAG laser operating at a pulse rate of 10 Hz with 10 nsec pulse lengths. The laser optical frequency could be adjusted over a 30 GHz bandwidth by changing the control voltage of the injection seeder. Each optical receiver consisted of a polarization insensitive beam splitter, an Iodine vapor cell, and two industry standard RS-170 CCD video cameras. The analog video signals were digitized using 10-bit frame grabbers installed in a network of PC-class computers.

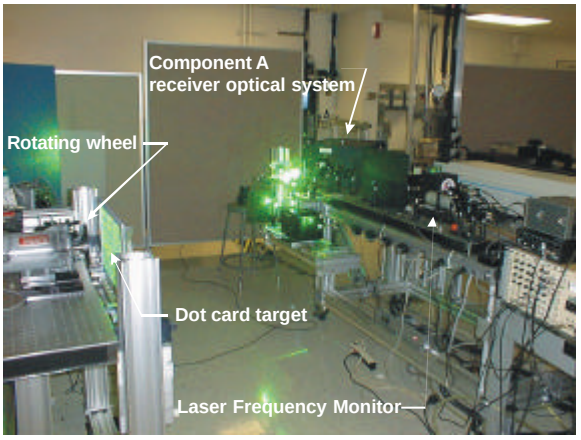

Fig. 1. Photograph of the laboratory setup.

The experiences during wind tunnel testing indicated that laser stability, drift in the Iodine vapor absorption line shape, laser speckle, and camera noise were potentially major sources of measurement error. The laboratory investigation addressed each of these areas in turn, and followed a logical progression to identify each source of error. Once the effects of each error source were understood, techniques were developed to minimize the contribution of that source to the error budget. Since the Iodine vapor absorption line characteristics serve as the transducer in DGV, this would be the logical starting point for the error source investigation.

3. IODINE VAPOR CELL CHARACTERISTICS

Two primary sources of measurement uncertainty are attributable to the Iodine vapor cells, the consistency of the absorption profile and the calibration of that profile. The optical absorption characteristics of Iodine vapor are dependent on the molecular number density. The greater the number of molecules, the wider and deeper each absorption line becomes. In addition, a general loss of transmission occurs for all optical frequencies, figure 2. For an evacuated sealed cell, the coldest temperature in the cell establishes the vapor pressure within the cell. If this temperature can be held constant, the absorption profile will also remain constant. Unfortunately, this dependency on temperature is very sensitive. The 0.1^{o} C uncertainty in the thermocouple / temperature controller results in a measurement uncertainty of 3 m/sec. Further, if the cell can not be totally isolated from large environmental temperature changes, the measurement uncertainty increases because of the inability of the

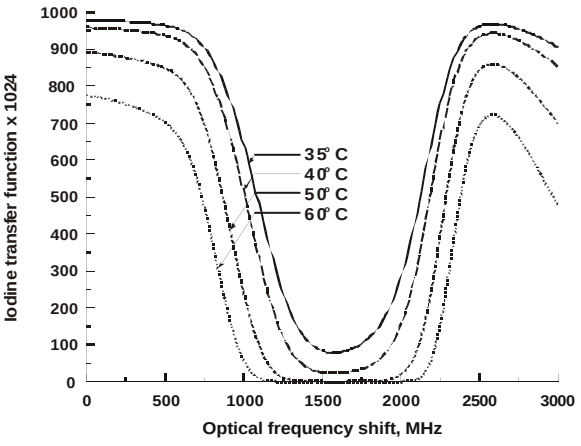

Fig. 2. A theoretical Iodine vapor absorption line profile as a function of temperature.

heating system to track large dynamic fluctuations.

Attempts to maintain a constant temperature within the cell using band heaters and insulated cases were successful in the laboratory. However, these cells failed in wind tunnel applications where the environmental temperature would change as much as 20° C during the day. Since the molecular density within the cells could not be maintained by controlling temperature, a different approach was needed.

The original Iodine vapor cells were constructed in keeping with the normal practices used in spectroscopy. A glass cell was purged with an inert gas, crystalline Iodine placed in the cell, and the cell evacuated. The desired absorption line characteristics could then be obtained by setting the temperature of the *cold finger* (a tube extending from the cell body) while keeping the body temperature high to prevent plating out of the Iodine on the body or cell windows. If Iodine vapor could be encased in the cell instead of crystalline Iodine, it may be possible to have a fixed molecular number density and thus maintain constant absorption line characteristics. The cell construction procedure was modified in an attempt to do this. A cell was constructed as stated above except the cold finger was lengthened and a stopcock added midway along the cold finger. The cold finger was then placed in a water bath set to 40° C and the cell allowed to stabilize for 24 hours. The stopcock was then closed and the cold finger welded shut between the stopcock and the body. Since the vapor pressure within the cell was established by the water bath, the absorption characteristics would remain the same regardless of temperature, provided the temperature was above the original 40° C. The absorption line profiles of this vapor-limited cell from 35° C to 60° C are shown in figure 3. The lack of temperature dependency is easily seen when compared to the profiles shown in figure 2.

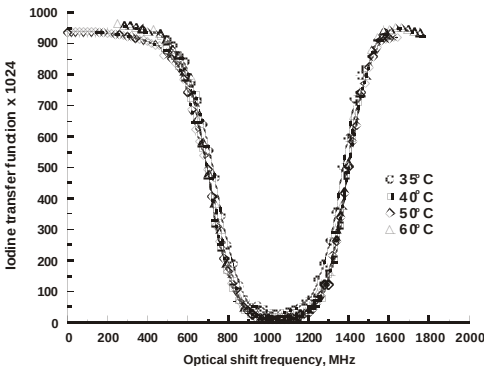

Fig. 3. Measured Iodine vapor absorption line profile for a vapor-limited cell set to a vapor pressure corresponding to 40° C.

Now that the absorption characteristics were stabilized, attention was shifted to the calibration of the profile. Standard practice in laser spectroscopy was to first calibrate the optical frequency tuning of the single-frequency, frequency-doubled Nd:YAG laser by determining the seeding injector control voltage settings for the centers of two adjacent absorption lines. Since the optical frequencies for the two absorption lines were known precisely, a linear relationship between the control voltage and optical frequency could be established. The absorption line profile could then be determined by measuring the transmission level of laser light through the cell while adjusting the control voltage to scan the laser frequency. Unfortunately there are two assumptions in this process that have been found to be in error. First, the relationship between the control voltage and the output laser frequency was not only found nonlinear, but nonrepeatable, figures 4 and 5. Further, the output frequency is not constant, but would vary up to 80 MHz from pulse to pulse while the control voltage remained constant, figure 4.

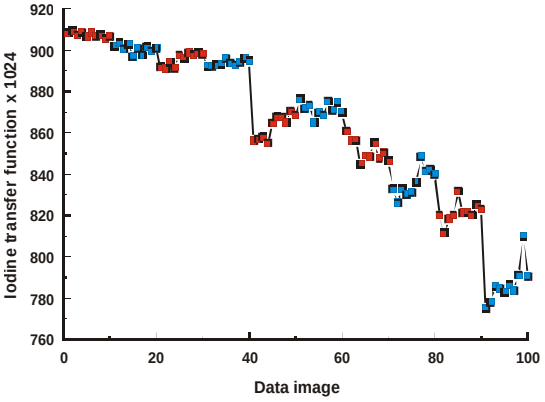

Fig. 4. Iodine vapor transfer function for each laser pulse, 10 pulses per injection seed laser control voltage setting.

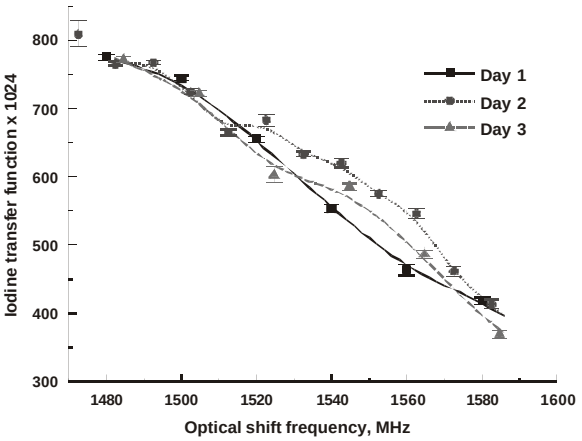

Fig. 5. Iodine vapor transfer function obtained by adjusting the injection seed laser control voltage, curve fit with a B-spline algorithm.

While this behavior prohibits the use of this technique, the investigation indicated that an external method might be used to determine the optical frequency of each laser pulse. The first approach tested was to monitor the shift of the fringe pattern generated by a Fizeau interferometer as the laser frequency was changed. This worked well in a macro sense, but did not provide the needed optical frequency resolution.

The second approach used the capabilities of DGV to measure the Doppler shift from a rotating wheel as an accurate source for a linear optical frequency distribution. The transmission optics were adjusted to produce a cone of light to illuminate the wheel which was located in the same horizontal plane as the transmission optical axis and the optical receiver system, figure 1. This configuration would produce a measure of the horizontal component of velocity from the wheel. Thus any vertical profile on the wheel would yield the same linear distribution of optical frequency. This distribution could be accurately defined by the rotational speed, as measured by an optical tachometer, and the Doppler shift equation:

$$\Delta n = \frac{n_o(\hat{o} - \hat{i}) \bullet V}{c}$$

where $\Delta\nu$ is the Doppler shift, ν_o is the laser frequency, V is the velocity of the wheel at the measurement point, $\hat{i}$ is the unit vector of the transmission light to the measurement point, $\hat{o}$ is the unit vector of the scattered light from the measurement point to the receiver, and c is the speed of light. The measurement of the signal/reference ratio along the vertical diameter would yield a segment of the absorption line profile. Thus, the absorption line profile could be accurately determined by combining the measured segments as the laser frequency was tuned through the absorption line. By shifting the overlapping adjacent segments along the frequency axis to minimize least square error, the segments could be joined to create the absorption profile without the knowledge of the laser frequency settings, figure 6. The repeatability of this technique coupled with the use of vapor limited cells is evident in figure 7, especially when compared to the same absorption line segment in figure 5.

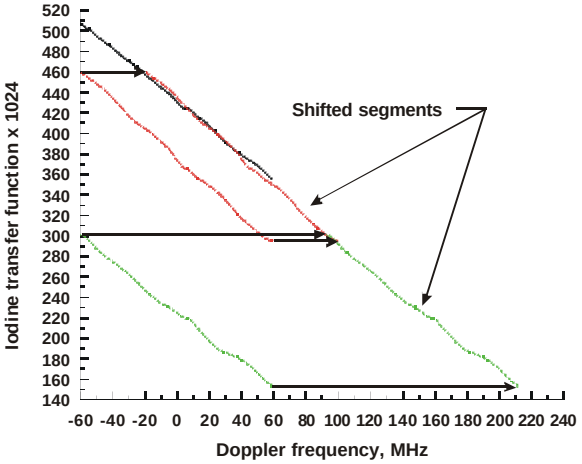

Fig. 6. Construction of the Iodine vapor absorption line calibration profile.

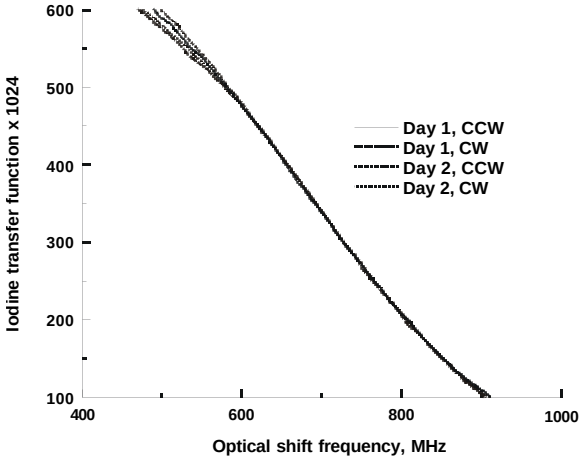

Fig. 7. Iodine vapor transfer function obtained by measuring the Doppler shift from a rotating wheel, no curve fit – data obtained every 0.28 MHz.

4. SIGNAL AMPLITUDE CONSIDERATIONS

Variations in signal amplitude resulting from the scattering of light from nonuniform particle number densities, polydisperse particle size distributions, and the nonuniform distribution of laser energy across the laser light sheet were recognized as problems in the original work described by Komine in his patent (Komine, 1990). These problems were solved by adding a reference camera to map the scattered energy distribution from the same area within the light sheet viewed by the signal camera. The signal image was then normalized by the reference image to produce an intensity map that was proportional to the flow velocity. If however, the distribution of collected light energy was modified along either the signal or reference optical path, an error would occur in the resulting normalized image. Potential contributors included background light, dirty optics, interferometric effects,

polarization effects, and drift in the video electronics. The primary effect caused by these contributors was a variation in the signal/reference ratio from the calibrated value for a given optical frequency.

Background light, whether from room lights, laser flare from the model or tunnel walls, or camera dark current represents an unknown offset in the collected light energy by the signal and reference cameras. Since the CCD video cameras are integrating devices, light energy originating from background sources adds directly to the collected scattered light energy from the particles. Thus background light can be eliminated by acquiring signal and reference images of the laser light sheet without the presence of seed particles. Subtracting these images from the signal and reference data images respectively would remove the influence of the background. It is also noted that new background images must be obtained if the test conditions change, causing a change in the background, e.g., change in the model angle of attack.

The remaining contributors influence the transmissivity through the signal and reference optical paths. Dirty optics have a direct blocking effect on light passing through the optical elements, thus lowering the strength of the collected scattered light for their respective optical path. Interferometric effects can be found in any laser application where light passes through an optical element with parallel faces, for example the windows on the Iodine vapor cell. The resulting fringe pattern will be a combination of linear fringes caused by the cell being slightly nonorthogonal to the optical axis and circular fringes from the slight bending of the cell windows caused by the vacuum inside the cell. The polarization of the collected scattered light becomes a contributor because the beam splitter used to direct the light down the signal and reference optical paths changes its reflection/transmission ratio with polarization angle. Even the *polarization insensitive* beam splitters have sufficient sensitivity to add a significant bias error to the velocity measurement. Finally, drift in the camera electronics gain, whether internal to the camera or external in the frame grabber will result in variations in the normalized value.

The common element among these contributions is their effect on the transmissivity of the signal and/or reference optics. For example assume that the beam splitter has a transmission/reflection ratio of 60/40 when the light is vertically polarized, but 50/50 when the light is horizontally polarized. Further, assume that the light scattered from the calibration wheel has the same Mie scattering characteristics as the seeding particles in the flow. However, the optical path taken by the laser beam to form the cone of light to illuminate the wheel for calibration of the Iodine vapor cells was considerably different than the path used to form the laser light sheet for flow measurements. These differences in optical path could easily result in a difference in the beam polarization orientation as it is scattered from the moving targets. Thus the signal/reference ratio obtained from the particle field could be considerably different than the calibration ratio for the same Doppler shifted frequency. To investigate the effects of polarization on the measurement, a Polaroid filter was placed in front of the optical receiver system and rotated to peak the transmission of the scattered light. After calibration of the Iodine absorption line, the filter was removed and a second calibration acquired. The second calibration had a similar shape, but only 82-percent of the amplitude of the

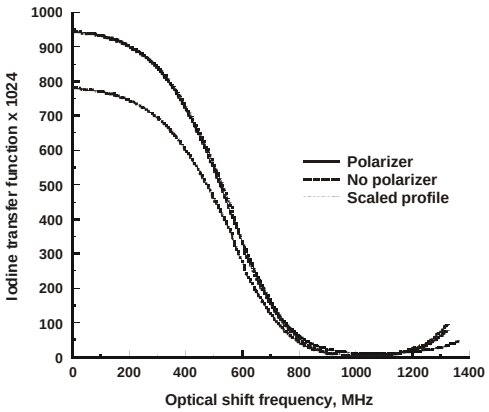

Fig. 8. Iodine vapor transfer function with and without a linear polarizer placed in front of the optical receiver system. Overlay plot is a gain adjust of the transfer plot obtained without the polarizer.

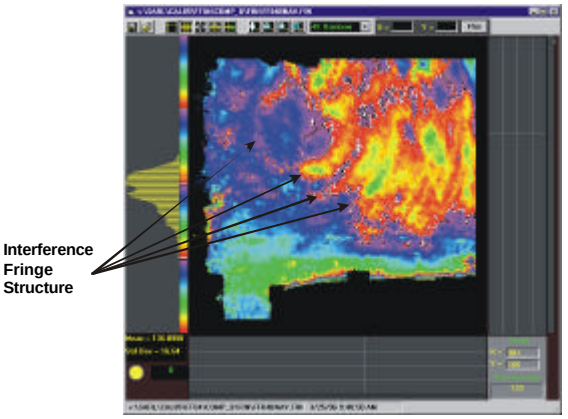

Fig. 9. An intensity flat field correction image containing interference fringes caused by the Iodine vapor cell windows.

first calibration indicating a different division of light by the beam splitter. The lower calibration was then scaled to match the peak of the first calibration to determine if the polarization effect was linear. The excellent comparison of the two calibrations shown in figure 8 verifies the linearity. Thus extending the measured ratio outside the absorption line to a fixed value, e.g., 1024, for the calibration wheel and the particle field will eliminate the polarization effect. In addition, this procedure also eliminates the effects of dirty optics, interferometric fringes, and drifting electronics, provided this intensity flat field is acquired periodically during testing to account for slow variations in transmissivity. This is accomplished by tuning the laser frequency outside the absorption line and acquiring a data set. An example intensity flat field is shown in figure 9.

5. HIGH FREQUENCY NOISE SOURCES

Noise is an ever-present condition in any electro-optic measurement system, and DGV is no exception. What is the exception is that noise in DGV occurs in two forms – spatial and temporal. Spatial noise is found in each camera image caused by laser speckle, variations in pixel sensitivity, charge transfer noise in the camera, and quantizing noise in the frame grabber. When the signal image is normalized by the reference image the influence of quantizing noise increases, especially at low signal levels. Variations in pixel amplitude from frame to frame are an additional source of noise that ultimately determines the minimum velocity resolution for a given pixel.

Countering the high frequency noise sources is the spatially low pass filtering effect of the Modulation Transfer Function (MTF). The optical component of the MTF is typically referred to as the *image sharpness*; e.g., an image obtained with a lens setting of f16 has a sharper focus than when obtained with a lens setting of f1.4. The electronic component of the MTF is typically referred to as *pixel bleed*; i.e., high levels of charge in a pixel will dissipate to adjacent pixels with lower charge. Typically the combined optical/electronic MTF has been found to be equivalent to approximately 5 pixels. Thus convolving the camera image with a 5x5 top hat kernel would reduce the effect of high frequency noise without affecting the data fidelity. This process is now routinely performed on the signal and reference images. Further, the normalized image is also filtered with the 5x5 kernel to help lower the quantizing effects amplified by the normalization.

The camera signal-to-noise ratio provides a measure of the minimum resolution obtainable with that camera. Typically signal-to-noise ratios are quoted based on electronic noise (or dark current) as compared with the maximum intensity measurable before saturation within a single image. This version of noise is greatly reduced by subtracting background and low pass filtering the images. However, frame-to-frame variations in the measured intensities remain a noise source. This temporal signal-to-noise can be increased by averaging a number of images provided the flow field is stationary. Images of a uniformly illuminated transparency containing a series of increasingly optically dense gray scale boxes, figure 10, were acquired to obtain a baseline temporal signal-to-noise ratio. Each camera / frame grabber acquired 100 images of the back-illuminated transparency. A 10-x 10-pixel subregion was selected from each of the 10 gray scale portions of the image. The mean and standard deviation were calculated for each pixel within the subregion throughout the 100 images. Each mean value represented the signal, and the standard deviation represented the noise. The resulting 100 signal-to-noise ratios were then averaged to obtain a measure of the camera signal-to-noise for that illumination level. The ten signal-to-noise ratios then formed the performance profile for the camera. Profiles were obtained from several camera / frame grabber combinations from an industry standard RS-170 analog camera using an 8-bit frame grabber up to a cooled 16-bit digital camera. The resulting profiles are shown in figure 11. The current DGV configuration uses an RS-

Fig. 10. Video camera calibration target.

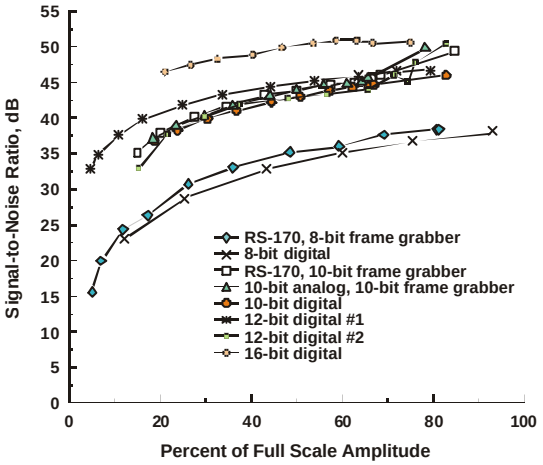

Fig. 11. Camera / frame grabber signal-to-noise response based on statistical noise obtained from 100 acquired images.

170 camera with a 10-bit frame grabber. This produces a resolution of 8.5 bits or an uncertainty of 1 part in 362. The cooled 16-bit camera produced a resolution of 9.5 bits or an uncertainty of 1 part in 724 at 28 times the cost of the current system.

6. OPTICAL CONSIDERATIONS

The optical system and its arrangement affect the measurement accuracy in several ways: signal strength, image distortion, depth of focus, and secondary scatter contamination. Optimizing these potential error sources is difficult, as they interact. For example, if the signal strength is low, opening the f-stop can increase it. However this decreases the depth of field and increases image distortion. Another method to increase signal strength is to add more particles to the flow. Unfortunately, this increases secondary scatter that adds uncertainty to the velocity measurement. In addition, other factors will influence the ability to minimize the total error budget, e.g., tunnel window location, structural blockage, potential laser energy, size of the light sheet, maximum particle number density, etc.

Signal strength is related to the laser power density, particle number density, particle size distribution, Mie scattering and the collecting solid angle of the receiver. Laser power is set by the choice of laser, and the area of interest sets the size of the laser light sheet. The particle number density is limited by the capabilities of the smoke generator and the aerodynamics controlling the size and location of the smoke plume. The smoke generator and the environmental conditions influencing the evaporation/ agglomeration of the particles establish the particle size distribution. The choice of viewing directions is usually a compromise between window location, desired light sheet plane, and sufficient angles among the measurement components to minimize trigonometric errors. It is suggested to keep the angle between each receiver and the light sheet greater than 30 degrees to limit the aspect ratio to less than 2:1. It is also suggested to keep the three measurement vectors greater than 45 degrees from each other. With these constraints, the effects of Mie scattering efficiency on signal strength usually become a secondary concern. Normally two receivers can be located to obtain efficient scattering, but the third is usually far less efficient. This lack of efficiency can sometimes be overcome by using a lens with a low f-number. This approach is limited by the diameter of the Iodine vapor cell and the potential for image distortion associated with short depth of field.

The signal and reference images are distorted by viewing perspective and minor imperfections in the optics and tunnel windows. Further, combining the three components on a pixel-by-pixel basis to obtain the standard orthogonal velocity components requires accurate overlay of the three component images. A piecewise, bilinear warping process was developed (Meyers, 1992) to eliminate these distortions from the data images. An example of the results obtained using this process is shown in figure 12. The spatial uncertainty of this warping process was investigated by Meyers and Lee (Meyers and Lee, 1999). The results from analytic simulation and measurement data at the edge of a rotating wheel, figure 13, indicate that the overlay spatial uncertainty was less than 0.07 pixels. This spatial uncertainty is the smallest error that can be detected since the 5-pixel wide impulse at the edge of the wheel, figure 13, is the narrowest impulse that can be measured because of the low pass effect of the camera MTF.

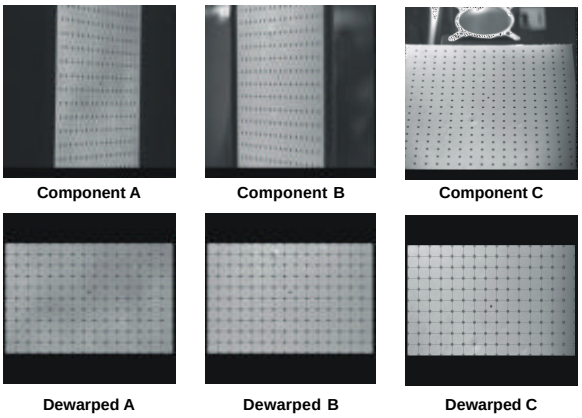

Fig. 12. Views of the image calibration target from the left, right, and above with an inclination angle of 30-degrees from the target plane before and after

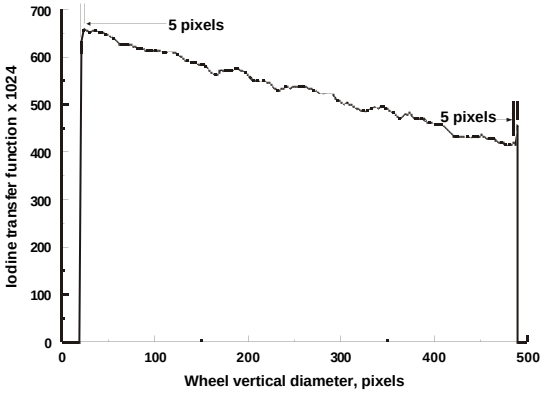

Fig 13. Normalized signal amplitude along the vertical axis of a rotating wheel indicating a misalignment of the signal and reference images.

The primary concern of a limited depth of field is the blurring of the image away from the center of focus. This can be thought of as the application of a variable sized kernel to low pass filter the image. The bandwidth of this filter would decrease with distance away from the center of focus. Thus flow details would be distorted or even lost through filtering as the distance from the center of focus increases. Further, combining a blurred image with sharp images from the other velocity components will produce inaccurate artifacts in the orthogonal velocity maps.

Since DGV is in essence a measure of collected scattered light energy, there is no way to differentiate the desired scattered light from particles passing through the light sheet and light originating from other sources. If the light sheet strikes the model or other structures viewed by the camera, this light can be eliminated as background. However, this light also illuminates the particle field, creating secondary scattered light whose optical frequency will not represent the flow velocity field passing through the light sheet. This process can also occur in reverse – light scattered by particles passing through the light sheet being reflected by the model. Röhle and Schodl (Röhle and Schodl, 1997) carry this process to particle-to-particle secondary scattering. While this contaminating effect can not be eliminated, its contribution can be lessened by painting the model and other viewed structures flat black or red, and keeping the seeding particle number density just high enough to yield efficient primary scattering.

7. LASER CONSIDERATIONS

A requirement of DGV is the use of a single frequency laser to produce green light that can be frequency tuned to match an Iodine absorption line. The two candidates are an Argon ion laser equipped with an etalon, and an injection seeded, frequency-doubled Nd:YAG laser. The Argon ion laser has the advantages of ease of operation, adjustable output power, and single frequency output stability. The Nd:YAG laser has the advantages of instantaneous measurement, high output power, and adjustable output frequency. Neither laser however, is sufficiently robust to operate properly in wind tunnel environments without significant isolation and monitoring. Temperature variations and structural vibrations will cause the lasers to change output frequency and even cease single frequency operation. Pressure changes may cause the lasers to cease operation altogether because of the resulting index of refraction changes within the optical cavity. Thus the laser must be isolated from the environment and the internal conditions monitored. Each laser pulse must also be monitored to determine if the laser is operating in single frequency mode, and the optical frequency measured to determine the Doppler shift measured in the data images.

The output frequency of an Argon ion laser can be set to the hyperfine structure along the Iodine vapor absorption line using appropriate feedback control systems, (Röhle and Schodl, 1997). Unfortunately, the output frequency from a Nd:YAG laser can not be locked to the hyperfine structure as the frequency can change as much as 80 MHz between successive pulses, figure 4. If the laser frequency can not be locked, it must be measured. A sample of the laser beam was obtained by directing a reflection from a glass block inserted in the beam path to a fourth optical receiver system. Although a simplified system could be constructed using photodiodes, the current Laser Frequency Monitor (LFM) was made identical to the component receiver systems, figure 1, to eliminate any potential problems with beam leakage outside the photodiode sensor region. Thus all four component data images are processed using similar software – the primary difference being the integration of the LFM signal and reference images before normalization. The component Doppler frequency maps could then be determined by simply subtracting the LFM frequency from each pixel value in the three data images.

The sensitivity of the lasers to environmental variations necessitates monitoring the laser for single frequency operation. The Argon ion laser is usually stable, but occasionally the frequency jumps from one longitudinal mode to the next. As the laser mode changes, both optical frequencies would occur during the camera integration time of 16.7 msec resulting in inaccurate velocity measurements. The laser frequency can be monitored using a scanning optical spectrum analyzer to interrogate a sample of the laser beam. If the analyzer shows a single, Gaussian shaped profile, the Argon ion laser is operating in single frequency mode. If the profile contains a secondary peak, the laser is oscillating between two adjacent modes and the data should be rejected until a single peak returns. The return to single frequency may occur spontaneously or it may require physical adjustment of the etalon.

The variation in optical frequency in the pulsed Nd:YAG output requires a method capable of determining whether each pulse is single frequency. This requirement eliminates the scanning optical spectrum analyzer. A flat plate interferometer was configured in the Fizeau mode to produce a parallel set of fringes that could be captured by a CCD array and interrogated by computer. The acquired image contains the mode structure and optical frequency of

the captured laser pulse. The interferometer worked well in determining single-frequency operation of the laser. However, the interferometer was extremely sensitive to vibration making it unusable in wind tunnel applications.

The characteristics of the Nd:YAG laser were studied while monitoring the flat plate interferometer in an attempt to find a parameter that would indicate single frequency operation. The most likely parameter was the Q-switch build up time. If the build up time (delay time between activation of the laser Q-switch and the output of the laser pulse) was short, the laser would produce a single frequency pulse. When the laser output became multimode, the build up time and the pulse duration increased. A monitoring system was constructed using a triggered boxcar integrator with a narrow, time delayed acceptance aperture. The Q-switch control pulse was used to trigger the boxcar integrator. The start of the acceptance aperture was set to match the delay found during single frequency operation. The boxcar integrator then integrated the signal obtained from a laser monitoring photodiode for a period of time matching the single frequency pulse duration. When the laser operated in single frequency, the integrated photodiode signal reached approximately 2.4 volts. When the laser became multimode, the delayed and widened pulse missed the acceptance aperture reducing the integrated voltage. Correlating the results with the flat plate interferometer and the measured Doppler shift from the rotating wheel suggested that integrated voltages greater than 1.9 volts indicated single frequency laser operation. The DGV data acquisition system was modified to measure the boxcar output and use the value as an acceptance criterion for each instantaneous data image. The monitoring capability of this approach is shown in figure 14 along with the measured Iodine transfer function. The effects on the measurements are easily seen when the laser shifts to multimode operation.

An unexpected characteristic of the Nd:YAG laser was found during the rotating wheel tests. The Iodine vapor absorption line transfer function was determined by aligning the measured normalized signal along the vertical diameter with the calculated Doppler frequency based on the rotational speed. When the wheel was spun in the opposite direction, the transfer function did not repeat as expected, figure 15. The normalized signal amplitudes matched outside the absorption line and at the bottom of the line, but the transitions were significantly different. Since the wheel rotational speed was set very accurately and the DGV system unchanged, the only possible explanation was that the laser beam contained a spatial variation in optical frequency. Forkey et al reported this possibility (Forkey et al, 1997), but only speculated as to its cause.

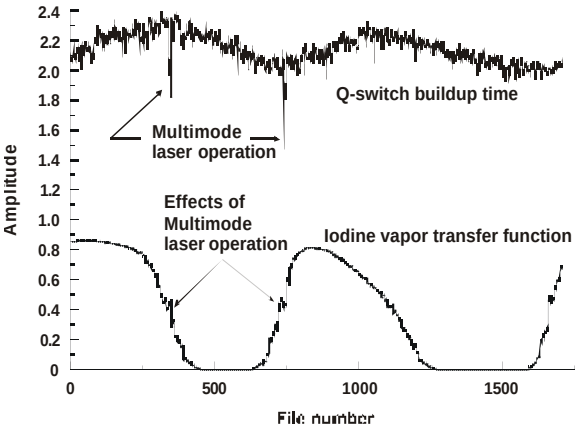

Fig. 14. Comparison of the Nd:YAG laser Q-switch buildup time with the Iodine vapor transfer function.

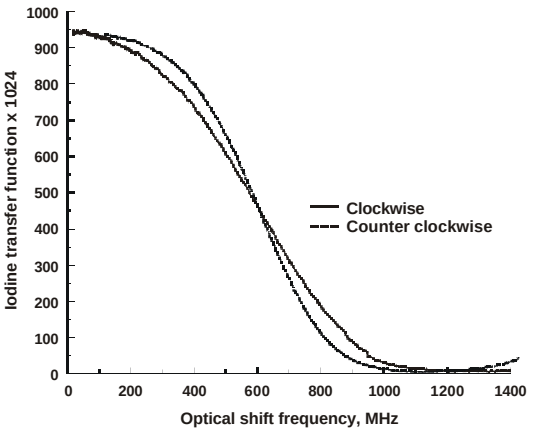

Fig 15. Iodine vapor transfer function obtained with the wheel rotating in the clockwise and counter clockwise directions.

The possibility of multiple output frequencies was traced to the physical characteristics of the Nd:YAG rods. These rods were constructed with the ends polished to a flatness of $\lambda/10$ and parallel to 10 arc seconds. The length of the rod could thus vary randomly 0.104 microns with a linear change of 0.291 microns. The number of cycles, q, maintained within the optical resonator cavity can be found from:

$$q = \frac{n_o\,(n_1 l_1 + n_2 l_2 + n_3 l_3)}{c}$$

where n_1, n_2, and n_3 are the index of refraction of each material, l_1, l_2, and l_3 are the length of the material, n_o is the laser frequency, and c is the speed of light. The first two elements are the two Nd:YAG rods: n = 1.823 and l = 0.1. The third element is air with n = 1.0 and l = 0.5. The distribution of optical frequency could be determined by lengthening one rod by 0.291 microns from top to bottom (the other rod was assumed to be perfect). This would also reduce the length of air by the same amount. Since the number of cycles supported within the optical resonator must be an integer number, the optical frequency supported must change as the rod length increases provided the frequency remains within the laser bandwidth, e.g., 120 MHz. Thus:

$$q = \frac{n_o\,(2nl + l_3)}{c} = \frac{n_1\,(n(2l+\Delta) + l_3 - \Delta)}{c}$$

Substituting the above values in the equation and solving for the difference between ν_o and ν_1 yields a frequency distribution of 78 MHz per rod. The flatness uncertainty would yield a potential frequency difference of 28 MHz per surface. These frequency uncertainties are significant and must be corrected.

The first approach was to use the images acquired by the LFM to obtain a *frequency* flat field. The ratio image obtained in the LFM would provide a direct measure of the frequency distribution within the laser beam. This distribution could then be adjusted to produce an image that would be subtracted from the data images to remove the frequency variations contained in the laser beam. Unfortunately, interferometric fringes present in the LFM images greatly overwhelm the frequency variations, thus eliminated this approach. A second approach used the differences found during the wheel tests to develop the frequency flat field. Back-to-back measurements were acquired with the wheel rotating first in the clockwise, then in the counter clockwise direction with the laser set to the linear portion of the Iodine absorption profile. Averaging the two resulting data images produced the proper Doppler frequency calibration. The difference between the two images produced an image proportional to the laser frequency distribution. Converting the difference image to frequency using the calibration obtained from the average produced the frequency flat field image.

Using the frequency flat field to correct the rotating wheel data proved successful, figure 16. The remaining minor variations indicate that the laser rods have not stabilized with temperature. A new calibration was obtained several hours later and applied to a new data set, figure 17. The reduced variations indicate that the laser has reached equilibrium. The least squares error along the vertical diameter reduced to 0.5 m/sec for the second data set.

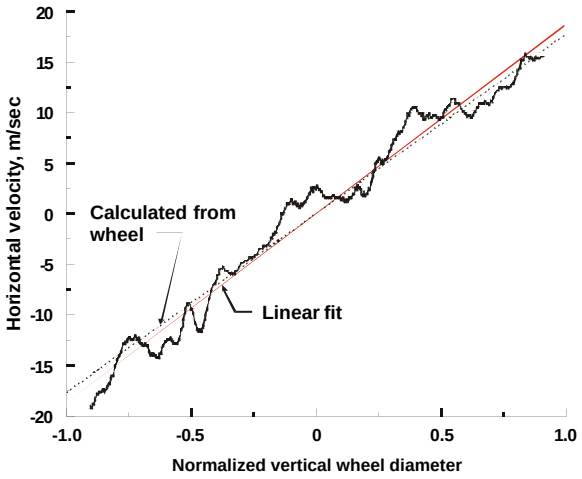

Fig. 16. Horizontal velocity profile along the vertical diameter of the rotating wheel, laser warm up – 1 hour.

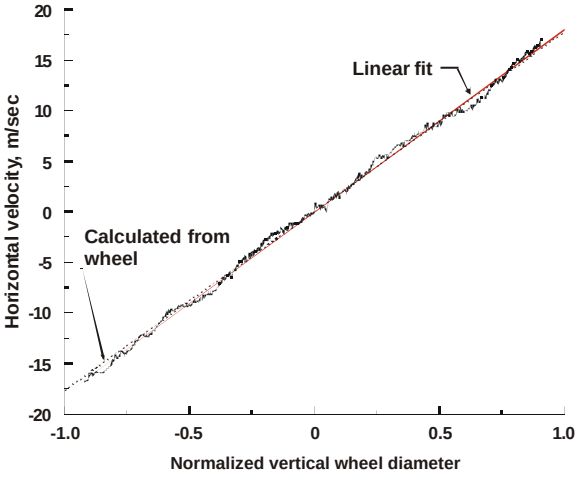

Fig. 17. Horizontal velocity profile along the vertical diameter of the rotating wheel, laser warm up – 4 hours.

8. PUTTING IT TOGETHER

The effectiveness of the above error reduction methods was tested by comparing DGV measurements of a jet flow exiting a fully developed turbulent pipe with Pitot probe measurements. The laser light sheet was orientated in a vertical plane angled 45 degrees to the flow axis with the sheet intersecting the centerline one radius from the end of the pipe. The optical receiver system was set orthogonal to the light sheet to directly measure the axial component of velocity. Since the light sheet was angled, only the vertical profile at the centerline of the pipe represented the flow velocity contour. The measured profile is compared with the Pitot measurements in figure 18. The small statistical uncertainty in the measured profile indicates that the measurement contains very little random noise. The variations in the DGV profile were caused by the frequency distribution within the laser beam. Corrective procedures for this error have yet to be developed for light sheet applications.

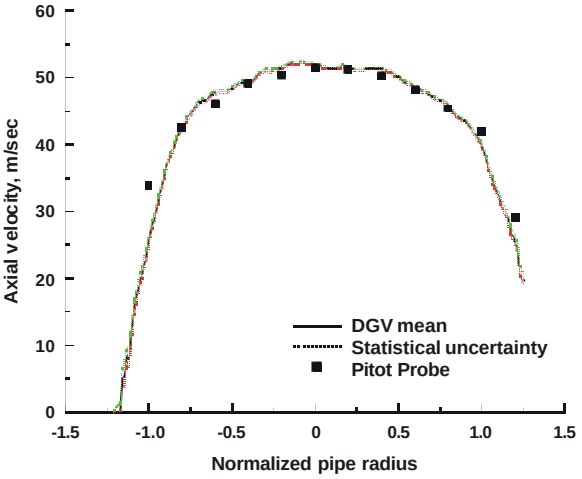

Fig. 18. Comparison of DGV velocity measurements of the jet flow exiting a fully developed turbulent pipe with Pitot probe measurements.

9. SUMMARY

An analysis of the technology comprising a Doppler Global Velocimetry measurement system has been presented. The primary goal of this analysis was the identification and minimization of measurement errors. The areas investigated were the Iodine vapor cell, signal amplitude biases and noise, optical factors, and the characteristics of the illuminating laser. The development of a vapor-limited Iodine vapor cell eliminated the effect of the environment on the absorption line transfer function. The accuracy of the calibration of this transfer function was greatly enhanced by using a rotating wheel to provide a known optical frequency distribution. The image warping procedures were shown to yield spatial uncertainties of 0.07 pixels. A Laser Frequency Monitor was constructed to measure the output frequency of each laser pulse, and a Q-switch monitoring system developed to determine if that pulse was a single frequency. Procedures to acquire intensity and frequency flat fields were developed and shown to reduce measurement uncertainties. These measurement error minimization techniques reduced the uncertainties to 0.5 m/sec. However, there remain problems with secondary scattering and the development of procedures to create a frequency flat field for laser light sheet applications.

REFERENCES

Forkey, J. N., Lempert, W. R. and Miles, R. B. (1997). "Observation of a 100-MHz frequency variation across the output of a frequency-doubled injection-seeded unstable-resonator Q-switched Nd:YAG laser", Optics Letters, vol. 22, no. 4, February 15, 1997.

Komine, H. (1990). "System for Measuring Velocity Field of Fluid Flow Utilizing a Laser -Doppler Spectral Image Converter", US Patent 4,919,536.

Meyers, J. F. and Komine, H. (1991). "Doppler Global Velocimetry - A New Way to Look at Velocity", Laser Anemometry: Advances and Applications, 1991, eds. A. Dybbs & B. Ghorashi, ASME, pp. 289-296.

Meyers, J. F. (1992). "Doppler Global Velocimetry – The Next Generation?", AIAA 17th Aerospace Ground Testing Conference, Nashville, TN, paper AIAA 92-3897, July 6-8, 1992.

Meyers, J. F. (1994). "Development of Doppler Global Velocimetry for Wind Tunnel Testing", AIAA 18th Aerospace Ground Testing Conference, Colorado Springs, CO, paper AIAA 94-2582, June 1994.

Meyers, J. F., Fleming, G. A., Gorton, S. A. and Berry, J. D. (1998). "Instantaneous Doppler Global Velocimetry Measurements of a Rotor Wake: Lessons Learned", Ninth International Symposium on Applications of Laser Techniques to Fluid Mechanics, paper 1.1, Lisbon, Portugal, July 13-16, 1998.

Meyers, J. F. and Lee, J. W. (1999). "Investigation of Measurement Errors in Doppler Global Velocimetry", SAE World Aviation Congress and Exposition, paper 1999-01-5599, San Francisco, CA, October 19-21, 1999.

Röhle, I. and Schodl, R. (1994). "Evaluation of the Accuracy of the Doppler Global Technique", Proceeding, Optical Methods and Data Processing in Heat and Fluid Flow, pp. 155-161, London, April 14-15, 1994.

Röhle, I. and Schodl, R. (1997). "Applications of three dimensional Doppler global velocimetry to turbo machinery and wind tunnel flows", Proceeding, 7th Intl. Conf. On Laser Anemometry Advances and Applications, pp. 387-395, Karlsruhe, Germany, 1997.

Usry, J. W., Meyers, J. F. and Miller, L. S. (1992). "Doppler Global Velocimeter Measurements of the Vortical Flow above a Thin Delta Wing", AIAA 30th Aerospace Sciences Meeting and Exhibit, paper AIAA-92-0005, Reno, NV, January 6-9, 1992.